멤브레인(Membrane Journal)
Vol. 34 No. 5 October 2024, 253-261

Print ISSN: 1226-0088
Online ISSN: 2288-7253
DOI: https://doi.org/10.14579/MEMBRANE_JOURNAL.2024.34.5.253

# 이산화탄소 포집 및 탄산염 전환 통해 제조된 $FeCO_3$/rGO 복합체: 리튬이온 전지향 고성능 음극재

이 상 림*,1 · 구 가 휘*,1 · 박 대 웅* · 임 휘 윤* · 이 용 재* · 문 준 석* · 신 원 호** · 손 희 상*,†

*광운대학교 화학공학과, **광운대학교 전자재료공학과
(2024년 9월 30일 접수, 2024년 10월 15일 수정, 2024년 10월 15일 채택)

# $FeCO_3$/rGO Composites Prepared by $CO_2$ Capture and Carbonate Conversion: Anode Material in Lithium-Ion Batteries with Enhanced Performance

**Sanglim Lee*,1, Gahwi Gu*,1, Daeung Park*, Hwiyun Im*, Yongjae Lee*, Junseok Moon*, Weonho Shin**, and Hiesang Sohn*,†**

*Department of Chemical Engineering, Kwangwoon University, Seoul 01897, Republic of Korea
**Department of Electronic Material Engineering, Kwangwoon University, Seoul 01897, Republic of Korea
*(Received September 30, 2024, Revised October 15, 2024, Accepted October 15, 2024)*

요 약: 탄소중립을 달성하기 위해 이산화탄소를 포집, 활용, 저장하는 CCUS (carbon capture, utilization, and storage) 기술이 주목받고 있다. 본 연구에서는 광물 탄산화 공정을 통해 이산화탄소를 탄산염으로 고정하고, 이를 전이금속 탄산염 기반 리튬이온배터리 (LIB) 음극재로 적용하였다. $CO_2$를 탄산염으로 고정후, 이를 이용해 $FeCO_3$를 제작하고, rGO와 PVP와 복합화하여 음극활물질에 적용하였다. rGO는 전기전도도를 높이고 입자의 응집을 방지해 부피 팽창을 완화했으며, PVP는 계면활성제로서 입자 표면을 안정화하여 구조적 안정성을 강화하였다. $FeCO_3$-PVP-rGO 복합체 기반한 음극재에 대한 전기화학 테스트를 진행한 결과, $FeCO_3$/rGO 복합체는 1,620 mA/g의 전류 밀도에서 50 사이클 이후에도 400 mAh/g의 용량을 유지하였다. 본 연구는 $CO_2$를 고부가가치 배터리 소재로 전환하여 차세대 에너지 저장 기술에 기여할 가능성을 시사한다.

**Abstract:** Carbon capture, utilization, and storage (CCUS) technology is gaining attention as a key strategy for achieving carbon neutrality. In this study, $CO_2$ was permanently fixed as carbonate through mineral carbonation and applied as an anode material for lithium-ion batteries (LIBs). Such a fixed carbonate by $CO_2$ was used for the preparation of $FeCO_3$ composited with rGO and PVP to be applied as active material for negative electrode in LIBs. Specifically, the rGO plays an important role to increase electrical conductivity and prevent particle aggregation while PVP could stabilize the particle surface and strengthened structural stability as a surfactant. Electrochemical tests showed that the LIB anode material based on $FeCO_3$/rGO composite maintained a capacity of 400 mAh/g after 50 cycles at a current density of 1,620 mA/g. This study suggests the converting $CO_2$ into valuable battery materials can contribute to future energy storage technologies.

***Keywords:*** *lithium ion battery, $CO_2$ capture, $FeCO_3$, anode, rGO*

## 1. Introduction

The drastic climate change and environmental pollution have become globally significant issue[1-3]. Carbon dioxide ($CO_2$) emissions from industrial processes have been identified as one of the major causes of global warming[4-5]. Therefore, it is crucial to develop technologies that can capture and convert $CO_2$ into useful substances. carbon capture and utilization (CCU) and carbon capture, utilization, and storage (CCUS) technologies have gained attention for storing $CO_2$ in a stabilized form by converting it into useful

[1] The authors equally contributed to this work.
†Corresponding author(e-mail: sonisang@hanmail.net; http://orcid.org/0000-0002-4164-9397)

materials. Specifically, mineral carbonation technology is an effective method to convert $CO_2$ into chemically stable storage form of carbonates with high environmental safety[6-9].

Graphite, the conventional anode material for lithium-ion batteries (LIBs), has a limited energy density due to its low theoretical capacity of 372 mAh/g, facing to be changed with alternative anode material with high capacity including metal oxide, Si and lithium [10-20]. Among them, transition metal carbonates have been highlighted as the potential alternative anode to significantly improve LIB performance due to their high reversible capacity. However, the existing transition metal carbonate anodes failed to be commercialized due to its low electrical conductivity and volume expansion, hindering their practical application towards LIB anode with high electrochemical performance[21-23].

In this regards, iron carbonate ($FeCO_3$) is an appropriate transition metal carbonate for LIB anode. Specifically, $FeCO_3$ is low-cost and non-toxic material which can be prepared by $CO_2$ conversion. However, the practical application of iron carbonate towards LIB anode is limited by its poor electrochemical performance due to low electrical conductivity and volume expansion of $FeCO_3$[24-26].

In this study, we report a novel CCUS technology including mineral carbonation of $CO_2$ to be utilized as LIB anode material through simple and facile process. Briefly, we first prepare $FeCO_3$ by serial process of $CO_2$ capture and sodium carbonate conversion followed by metathesis. For the enhancement of conductivity and volume expansion of $FeCO_3$, a composite of reduced graphene oxide (rGO) and polyvinylpyrrolidone (PVP) and $FeCO_3$ was prepared through hydrothermal process and high temperature sintering. The material and electrochemical properties of the synthesized nanocomposites were analyzed to evaluate the applicability of nanocomposite towards LIB anode.

## 2. Experimental

### 2.1. Materials

Sodium hydroxide (NaOH, 99.5%), sodium chloride (NaCl, 99.0%), L-ascorbic acid ($C_6H_8O_6$, AA, 99.0%), ethylene gylcol (EG, 99.5%), hydrochloric acid (HCl, 35.0%), sulfuric acid ($H_2SO_4$, 95.0%), potassium permanganate ($KMnO_4$ 99.3%), hydrogen peroxide ($H_2O_2$, 30.0%) were purchased from Duksan Chemical. Iron(III) chloride hexahydrate ($FeCl_3$ $6H_2O$, 99.0%), graphite (99%), phosphoric acid ($H_3PO_4$, 85.0%), ethyl ether (99.0%) were purchased from Daejung chemical. All materials were used as-received for synthesis without further purification.

### 2.2. Synthesis of sodium carbonate through mineral carbonation

The sodium carbonate was prepared through carbonation and low-temperature crystallization with 2M NaOH under a constant temperature (35°C). The initial pH of the NaOH solution was approximately 14 while $CO_2$ (95 vol.%, 200 cc/min) was then injected into the NaOH solution until the pH of solution reached to 11. After the $CO_2$ injection, the reactor temperature was lowered to 10°C for the facilitated $CO_2$ conversion into bicarbonate and carbonate ions. The injection of $CO_2$ was continued for the crystallization at 2°C until the pH of the mixture reached to 7. After the crystallization, the white precipitate was formed in the solution and was separated through filtration.

The overall chemical reaction for $Na_2CO_3$ formation can be described as follows:

Initial reaction with NaOH to form sodium bicarbonate:

$$NaOH + CO_2 \rightarrow NaHCO_3 \quad (1)$$

Further reaction of sodium bicarbonate with NaOH to form sodium carbonate:

$$NaHCO_3 + NaOH \rightarrow Na_2CO_3 + H_2O \quad (2)$$

In this experiment, 10.2 g of $CO_2$ was injected into the NaOH solution, leading to the formation of 8.1 g of $Na_2CO_3$. Considering the molar weights of $CO_2$ and $Na_2CO_3$, and assuming a 1:1 molar conversion ratio, the theoretical $Na_2CO_3$ yield was calculated. The actual yield achieved, 8.1 g, corresponds to a percentage yield of approximately 32.9%. These data provide a quantitative measure of the $CO_2$ conversion efficiency under these experimental conditions and indicate that around 1.26 g of $CO_2$ is required to produce 1 g of $Na_2CO_3$.

### 2.3. Synthesis of $FeCO_3$/rGO composite

For the preparation of $FeCO_3$/rGO composite, the previously synthesized sodium carbonate was used as a carbonate precursor to be mixed with graphene oxide. Specifically, graphene oxide (GO) dispersed in the distilled water was mixed with the solution of $FeCl_3$ in an ethylene glycol (EG)-water mixture (1:1 volume ratio). Then, ascorbic acid (AA) and polyvinylpyrrolidone (PVP) were subsequently added to the mixed solution of GO and $FeCl_3$ for the preparation of precursor for the subsequent hydrothermal synthesis. The as-prepared precursor was transferred to a teflon-lined autoclave to be synthesized as $FeCO_3$/GO composite at 180°C for 12 hours. In the end, $FeCO_3$/rGO composite can be prepared by high temperature reduction by sintering at 500°C for 4 hours under a nitrogen ($N_2$) atmosphere.

### 2.4. Material characterization

The crystal structure and chemical composition of the sodium compound, $FeCO_3$, and $FeCO_3$/rGO composite were characterized with physical and chemical analytical instruments. The crystal structure of the material was analyzed by X-ray diffractometer (XRD, Rigaku) at a $2\theta$ range of 20~60° using CuK$\alpha$ (= 0.154059 nm) as radiation source. Surface chemical functionality (chemical bonds and molecular vibrations) for materials were analyzed mounted on ZnSe crystal at a wavenumber range of 750~2500 nm with Fourier Transform Infrared Spectroscopy (FT-IR, JASCO). The morphological information of the materials were obtained with Scanning Electron Microscopy (FE-SEM, Hitachi) using a secondary electron detector (SE) under an acceleration voltage of 5 kV and a working distance of 8 mm.

### 2.5. Electrochemical characterization

The electrochemical properties of the material was characterized by analyzing their symmetric cell performance and electrochemical impedance spectroscopy (EIS). The cell electrodes was prepared with pasted slurry mixtures of the active material, Super P, and PVDF at 7:2:1 on the Cu foil. The as-prepared cell electrode was then cut into discs and assembled to coin type electrochemical cells containing lithium foil, separator (celgard 2400), and electrolytes (1 mol/L $LiPF_6$ in ethylene carbonate (EC)/dimethyl carbonate (DMC)). Galvanostatic cycling tests were conducted using a battery tester (WBCS3000, Wonatech) system over the voltage range of 0.01~3.0 V. Electrochemical impedance spectroscopy (EIS) was performed in the frequency range 100 kHz to 0.1 Hz with a potentiostat.

## 3. Results and Discussion

### 3.1. Material characterization

Fig. 1. displays the crystal structure of $FeCO_3$ and $FeCO_3$/rGO composite. All the peaks of the samples can be indexed into rhombohedral $FeCO_3$ (R3c space group, PDF Card No.: 5000036). Different from the characteristic peaks of $FeCO_3$, a weak and broad band of $FeCO_3$/rGO suggests the presence of rGO due to the decreased crystallinity and a reduced grain size of $FeCO_3$[28]. As-calcuated grain sizes for $FeCO_3$ and $FeCO_3$/rGO are estimated to be 7.82 and 2.31 nm, respectively, attributing to the suppressed aggregation of $FeCO_3$ nanoparticles uniformly distributed on the rGO nanosheets[29].

Fig. 2 shows the FT-IR spectra of $Na_2CO_3$ prepared by $CO_2$ capturing and $FeCO_3$ synthesized using $Na_2CO_3$ as a carbonate precursor. As shown in the FT-IR spectra, strong absorption peaks at 1,390 $cm^{-1}$ and 880 $cm^{-1}$ observed in $Na_2CO_3$, indicates the

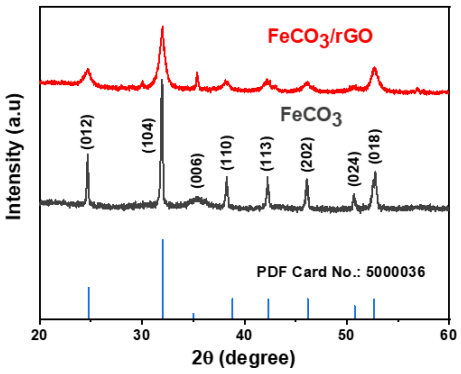


**Fig. 1.** Crystal structure analyses: XRD patterns of $FeCO_3$ and $FeCO_3$/rGO composite.

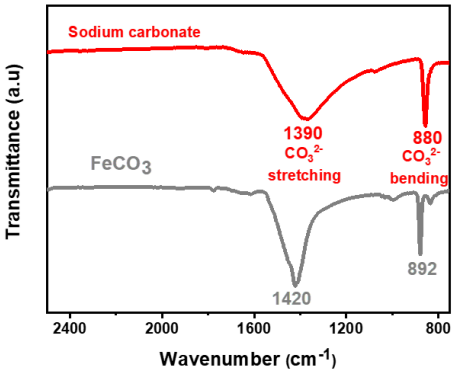


**Fig. 2.** Surface chemical functionality analyses: FT-IR spectra of sodium carbonate ($Na_2CO_3$) and iron carbonate ($FeCO_3$) synthesized via mineral carbonation.

stretching and bending vibrations of $CO_3^{2-}$, indicating the successful carbonate ions formation of $Na_2CO_3$ [13]. Similarly, strong absorption peaks at 1,420 $cm^{-1}$ and 892 $cm^{-1}$ observed in $FeCO_3$ can be assigned to $CO_3^{2-}$, indicating the carbonate ions formed in $FeCO_3$, similarly with that of $Na_2CO_3$[19]. As demonstrated in the chemical functionality of materials, the successful $CO_2$ capturing have been performed through the effective storage as carbonate form and subsequently converted to $FeCO_3$[30].

As displayed in the Fig. 3, the morphological structure of as-synthesized $FeCO_3$ and $FeCO_3$/rGO composite were analyzed with scanning electron microscopy (SEM). As shown in Fig. 3a, as-synthesized $FeCO_3$ microparticles by the solvothermal process are visible to have an irregular shape with the size of ca. 5~7

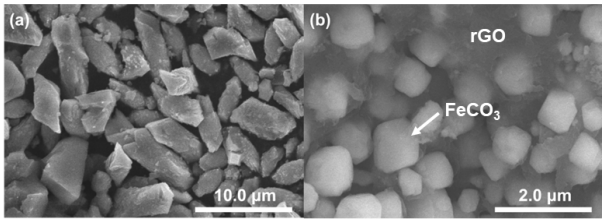


**Fig. 3.** Morphological analyses: SEM images of (a) $FeCO_3$ microparticles and (b) $FeCO_3$/rGO nanocomposites.

μm. As for the morphology for the rGO/$FeCO_3$ composite (Fig. 3b), as-formed $FeCO_3$ nanoparticles are observed as particles homogeneous distributed on rGO nanosheet with a mitigated size of 500~800 nm [31]. Such the different size and morphology of $FeCO_3$/rGO composite from that of $FeCO_3$ is attributed to the controlled growth of $FeCO_3$ nanoparticles in the rGO based composite matrix[15].

### 3.2. Electrochemical analysis

Fig. 4 compares the electrochemical properties for $FeCO_3$ and $FeCO_3$/rGO composite as the anode for lithium ion battery, As displayed in voltage profiles (Fig.s 4(a) and 4(b)) for charge/discharge at various cycles (1st, 2nd, 10th, and 50th cycles) at 1.62 A/g and 0.01 to 3 V, the large irreversible capacity losses are observed for $FeCO_3$ (1,325 mAh/g→747 mAh/g) and the $FeCO_3$/rGO composite (1,490 mAh/g→908 mAh/g) at the initial and second cycles due to the solid electrolyte interface (SEI) film formation and and the degradation by the irreversible electrolyte/electrode reactions[11-18]. As-formed SEI and irreversible reactions reduce the available capacity for subsequent cycles by consumption of lithium ions[32]. Specifically, the declined plateaus are observed in the first discharge for the $FeCO_3$ (from 0.71 V to 0.43 V) and for the $FeCO_3$/rGO composite (from 0.78 V to 0.53 V) attributed to the iron reduction ($Fe^{2+}$ to metallic $Fe^0$), and carbon reduction ($C^{4+}$ to $C^0$)[32]. As shown in the voltage profiles, the plateau curve above 0.5 V indicates the SEI layer formation in the composite[33]. Note that, the diminished plateau with stabilized voltage profile after 10 cycles suggests the reversible elec-

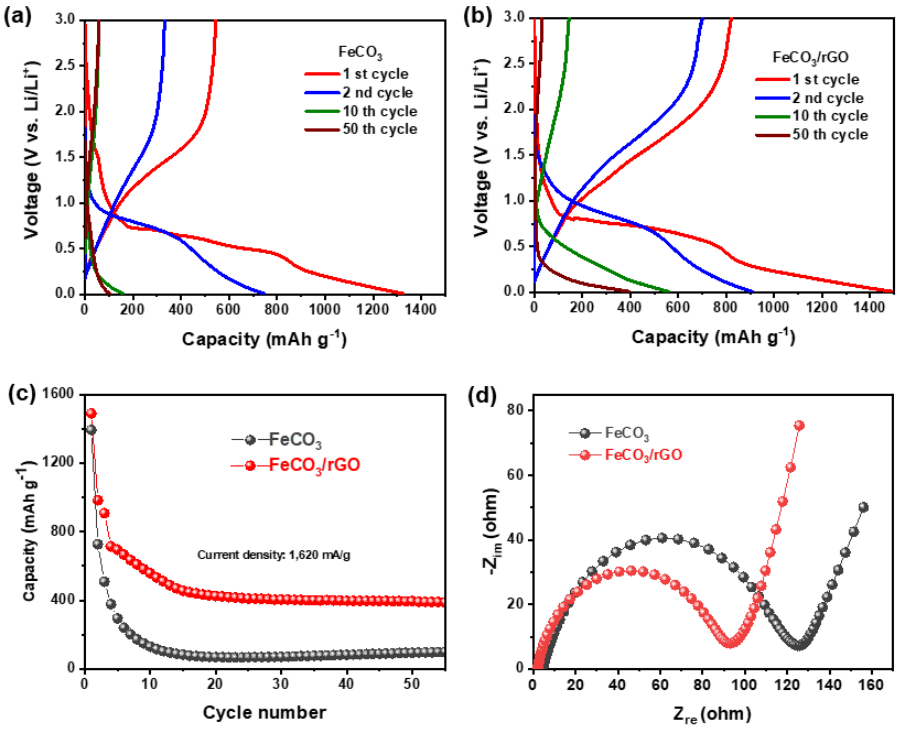


**Fig. 4.** Discharge/charge voltage profiles: (a) $FeCO_3$ (b) $FeCO_3$/rGO composite; (c) Cycling performance of $FeCO_3$ and $FeCO_3$/rGO composite; (d) EIS curves of $FeCO_3$ and $FeCO_3$/rGO composite.

trochemical reactions leading to the improved long-term cycle stability[34-35]. Furthermore, although the charge/discharge profiles show gradually decreased capacity at the elongated cycles (10th and 50th cycles) for both $FeCO_3$ and $FeCO_3$/rGO composites, $FeCO_3$/rGO composite displays much improved electrochemical performance compared to that of $FeCO_3$. Specifically, $FeCO_3$/rGO composite shows 557 mAh/g in the 10th cycle while the pristine $FeCO_3$ exhibits a capacity reduction to 159 mAh/g at the identical condition, indicating the more stabilized SEI layer and the reduced irreversible reactions of $FeCO_3$/rGO composite without continuous consumption of lithium ions [15-19]. Note that, $FeCO_3$/rGO composite shows the retained capacity (396 mAh/g) at elongated cycle (50th cycle) superior to that of $FeCO_3$ (103 mAh/g) at identical condition. Such the better capacity retention (cycle stability) of $FeCO_3$/rGO composite than that of pristine $FeCO_3$ indicates the mitigated structure degradation of $FeCO_3$ in the rGO composite due to structural stability and enhanced electronic conductivity by rGO nanosheet[17].

Fig. 4(c) compares the electrochemical performance (cycling stability and capacity) of $FeCO_3$ and $FeCO_3$/rGO composite. The $FeCO_3$/rGO nanocomposite exhibited the retained capacity (ca. 395 mAh/g) after 50 cycles, much superior to that of pristine $FeCO_3$ (95 mAh/g) at identical condition. Such the significantly improved performance (cycle stability and capacity retention) of the $FeCO_3$/rGO composite suggests effectively alleviated strain induced from $FeCO_3$ volume change and enhanced conducitivity of composite by introduction of rGO in to composite.

As displayed in Fig. 4(d), the resistance of the samples were compared with electrochemical impedance spectroscopy (EIS) analyses. The semicircle observed in high-frequency corresponds to the charge- transfer resistance ($R_{ct}$). As displayed in the EIS results, $FeCO_3$/rGO composite exhibit much lower resistance ($R_{ct}$, 93.09 $\Omega$) than that of bare $FeCO_3$ (121.62 $\Omega$), indicating facilitated charge transfer and improved ion

**Table 1.** Comparison of Anode Materials

| Samples | Capacity | Cycle | Ref. |
|---|---|---|---|
| $FeCO_3$-PVP-rGO | 395 mAh/g | 50 | This work |
| $FeCO_3$/rGO | 260 mAh/g | 80 | [31] |
| $CoCO_3$ | 266 mAh/g | 100 | [36] |
| $Al_2O_3$ coated graphite | 335 mAh/g | 100 | [37] |
| GO-$Mn_3O_4$ | 174 mAh/g | 40 | [38] |
| Structured graphite | 233 mAh/g | 100 | [39] |
| $N_2$+$H_2$ plasma modified graphite | 185 mAh/g | 500 | [40] |
| $AlF_3$ coated graphite | 150 mAh/g | 20 | [41] |
| CNT fabric | 305 mAh/g | 30 | [42] |
| Hard Carbon | 290 mAh/g | 100 | [43] |

mobility in the composite electrode[35].

## 4. Conclusion

In this study, we demonstrated a composite of $FeCO_3$ and rGO by carbonate based $CO_2$ capture/conversion and subsequent metathesis into $FeCO_3$ and rGO compositing to be applied as an anode material for LIBs.

As-prepared composite of $FeCO_3$ and rGO exhibited a superior electrochemical performance (retained cycle stability and capacity (400 mAh/g) after 50 cycles at 1.62 A/g) as LIB anode to that of pristine $FeCO_3$ based LIB anode (95 mAh/g) under the same test condition by overcoming the limitations of conventional transition metal carbonate anodes with the enhanced conductivity and alleviated strain of composite via introduction of rGO nanosheets. In addition, the $FeCO_3$/rGO composite exhibited a lower charge transfer resistance ($R_{ct}$) of 93.1 $\Omega$ than that for bare $FeCO_3$ (121.6 $\Omega$), suggesting enhanced electron mobility and ionic conductivity of our composite.

As-demonstrated in this report, our study highlights the potential of wasted $CO_2$ utilization to address environmental issues (carbon neutrality) by $CO_2$ conversion into high-valued LIB materials[34].

## Acknowledgement

This work was supported by Korea Electric Power Corporation (KEPCO) (Grant Number: R22XO05-09) and an NRF grant funded by the Ministry of Science and ICT (MSIT) of Korea (grant number NRF-RS-2023-0022 2124).

## Reference

1. P. A. Owusu and S. Asumadu-Sarkodie, “A review of renewable energy sources, sustainability issues and climate change mitigation”, *Cogent Eng.*, **3**, 1167990 (2016).
2. T. Dietz, R. L. Showom, and C. T. Whitley, “Climate change and society”, *Annu. Rev. Sociol.*, **46**, 135-158 (2020).
3. G. A. Florides and P. Christodoulides, “Global warming and carbon dioxide through sciences”, *Environment Inter.*, **35**, 390-400 (2009).
4. A. C. Köne and T. Büke, “Forecasting of $CO_2$ emissions from fuel combustion using trend analysis”, *Sustainable Energy Rev.*, **14**, 2906-2915 (2010).
5. E. Benhelal, G. Zahedi, E. Shamsaei, and A. Bahadori, “Global strategies and potentials to curb $CO_2$ emissions in cement industry”, *J. Cleaner Prod.*, **51**, 142-161 (2013).

6. P. Nejat, F. Jomehzadeh, M. M. Taheri, M. Gohari, and M. Z. A. Majid, "A global review of energy consumption, $CO_2$ emissions and policy in the residential sector (with an overview of the top ten $CO_2$ emitting countries)", *Renew. Sustainable Energy Rev.,* **43**, 843-862 (2015).
7. E. I. Koytsoumpa, C. Bergins, and E. Kakaras, "The $CO_2$ economy: Review of $CO_2$ capture and reuse technologies", *J. Supercritical Fluids*, **132**, 3-1 (2018).
8. E. S. Rubin, J. E. Davison, and H. J. Herzog "The cost of $CO_2$ capture and storage", *Inter. J. Greenhouse Gas Control*, **40**, 378-400 (2015).
9. L. Fu, Z. Ren, W. Si, Q. Ma, W. Huang, K. Liao, H. Huang, Y. Wang, J. Li, and P. Xu, "Research progress on $CO_2$ capture and utilization technology", *J. $CO_2$ Utilization*, **66**, 102260 (2022).
10. J.-W. Lee and W.-B. Kim, "Research trend of electrode materials for lithium rechargeable batteries", *J. Kor. Powder Metall. Inst.*, **21**, 473-479, (2014).
11. D. U. Park, W. H. Shin, and H. Sohn, "The enhanced electrochemical performance of lithium metal batteries through the piezoelectric protective layer", *Membrane J.*, **33**, 13 (2023).
12. J. H. Lim, J. H. Won, M. K. Kim, D. S. Jung, M. Kim, S.-M. Koo, J.-M. Oh, H. M. Jeong, C. Park, H. Sohn, and W. H. Shin, "Synthesis of flower-like manganese oxide for accelerated surface redox reactions on nitrogen-rich graphene of fast charge transport for sustainable aqueous energy storage", *J. Mater. Chem. A*, **10**, 7688 (2022).
13. Y. Jeong, J. Park, S. Lee, S. H. Oh, W. J. Kim, Y. J. Ji, G. Y. Park, D. Seok, W. H. Shin, J.-M. Oh, T. Lee, C. Park, A. Seubsaic, and H. Sohn, "Iron oxide-carbon nanocomposites modified by organic ligands: Novel pore structure design of anode materials for lithium-ion batteries", *J. Elec. Anal. Chem.*, **904**, 115905 (2022).
14. S. Lee, S.-S. Choi, J.-H. Hyun, D.-E. Kim, Y.-W. Park, J.-S. Yu, S.-Y. Jeon, J. Park, W. H. Shin, and H. Sohn, "Nanostructured PVdF-HFP/$TiO_2$ composite as protective layer on lithium metal battery anode with enhanced electrochemical performance", *Membrane J.*, **31**, 417 (2021).
15. K. Hwang, N. Kim, Y. Jeong, H. Sohn, and S. Yoon, "Controlled nanostructure of a graphene nanosheet-$TiO_2$ composite fabricated via mediation of organic ligands for high-performance Li storage applications", *Int. J. Energy Res.*, **2021**, 1 (2021).
16. D. Seok, W. H. Shin, S. W. Kang, and H. Sohn, "Piezoelectric composite of $BaTiO_3$-coated $SnO_2$ microsphere: Li-ion battery anode with enhanced electrochemical performance based on accelerated Li+ mobility", *J. Alloys Comp.*, **870**, 159267 (2021).
17. S. Lee, D. Seok, Y. Jeong, and H. Sohn, "Surface modification of Li metal electrode with PDMS/GO composite thin film: Controlled growth of Li layer and improved performance of lithium metal battery (LMB)", *Membrane J.*, **30**, 38 (2020).
18. Y. Jeong, D. Seok, S. Lee, W. H Shin, and H. Sohn, "Polymer/inorganic nanohybrid membrane on lithium metal electrode: Effective control of surficial growth of lithium layer and its improved electrochemical performance", *Membrane J.*, **30**, 30 (2020).
19. D. Seok, Y. Jeong, K. Han, D. Y. Yoon, and H. Sohn, "Recent progress of electrochemical energy devices: Metal oxide–carbon nanocomposites as materials for next-generation chemical storage for renewable energy", *Sustainability*, **11**, 3694 (2019).
20. K. B. Hwang, H. Sohn, and S. H. Yoon, "Mesostructured niobium-doped titanium oxide-carbon (Nb-$TiO_2$-C) composite as an anode for high-performance lithium-ion batteries", *J. Power Sources*, **378**, 225-234 (2018).
21. J. Li, M. Li, C. Guo, and L. Zhang, "Recent progress and challenges of micro-/nanostructured transition metal carbonate anodes for lithium ion batteries", *Eur. J. Inorg. Chem.*, **41**, 4508-4521 (2018).
22. M. Zhao, Y. Liu, J. Jiang, C. Ma, G. Yang, F. Yin, and Y. Yang, "Sheath/core hybrid $FeCO_3$/carbon nanofibers as anode materials for superior cycling

stability and rate performance", *ChemElectroChem*, **4**, 1450-1456 (2017).
23. M. Kwon, J. Park, and J. Hwang, "Conversion reaction-based transition metal oxides as anode materials for lithium ion batteries: Recent progress and future prospects", *Ceramist*, **25**, 2, 218-246, (2022).
24. L. Su, Z. Zhou, X. Qin, Q. Tang, D. Wu, and P. Shen, "$CoCO_3$ submicro cube/graphene composites with high lithium storage capability", *Nano Energy*, **2**, 276-282 (2013).
25. C. Zhang, W. Liu, D. Chen, J. Huang, X. Yu, X. Huang, and Y. Fang, "One step hydrothermal synthesis of $FeCO_3$ cubes for high performance lithium-ion battery anodes", *Electrochim. Acta*, **182**, 559-564 (2015).
26. X. Liu, H. Wang, C. Su, P. Zhang, and J. Bai, "Controlled fabrication and characterization of microspherical $FeCO_3$ and $\alpha$-$Fe_2O_3$", *J. Col. Interface Sci.*, **351**, 427-432 (2010).
27. F. Zhang, R. Zhang, J. Feng, L. Ci, S. Xiong, J. Yang, Y. Qian, and L. Li, "One-pot solvothermal synthesis of graphene wrapped rice-like ferrous carbonate nanoparticles as anode materials for high energy lithium-ion batteries", *Nanoscale*, **7**, 232-239 (2015).
28. K. H. Seng, M.-H. Park, Z. P. Guo, H. K. Liu, and J. Cho, "Catalytic role of Ge in highly reversible $GeO_2$/Ge/C nanocomposite anode material for lithium batteries", *Nano Lett.*, **13**, 1230-1236 (2013).
29. B. Yao, Z. J. Ding, X. Y. Feng, L. W. Yin, Q. Shen, Y. C. Shi, and J. X. Zhang, "Enhanced rate and cycling performance of $FeCO_3$/graphene composite for high energy Li ion battery anodes", *Electrochim. Acta*, **148**, 283-290 (2014).
30. S. Veerasingam and R. Venkatachalapathy, "Estimation of carbonate concentration and characterization of marine sediments by fourier transform infrared spectroscopy", *Infrared Phys. Technol.*, **66**, 136-140 (2014).
31. D. Xu, W. Liu, C. Zhang, X. Cai, W. Chen, Y. Fang, and X. Yu, "Monodispersed $FeCO_3$ nanorods anchored on reduced graphene oxide as mesoporous composite anode for high-performance lithium-ion batteries", *J. Power Sources*, **364**, 359-366 (2017).
32. Y. Huang, Y. Li, R. Huang, and J. Yao, "Ternary $Fe_2O_3$/$Fe_3O_4$/$FeCO_3$ composite as a high-performance anode material for lithium-ion batteries", *J. Phys. Chem. C*, **123**, 12614-12622 (2019).
33. M. Zhao, Y. Liu, J. Jiang, C. Ma, G. Yang, F. Yin, and Y. Yang, "Sheath/core hybrid $FeCO_3$/carbon nanofibers as anode materials for superior cycling stability and rate performance", *ChemElectroChem*, **4**, 1450 (2017).
34. X. Zhou, Y. Zhong, M. Yang, Q. Zhang, J. Wei, and Z. Zhou, "$Co_2(OH)_2CO_3$ nanosheets and CoO nanonets with tailored pore sizes as anodes for lithium ion batteries", *ACS Appl. Mater. Interfaces*, **7**, 12022-12029 (2015).
35. Y. Zhao, Y. L. Mu, L. Wang, M. J. Liu, X. Lai, J. Bi, D. J. Gao, and Y. F. Chen, "$MnCO_3$-RGO composite anode materials: In-situ solvothermal synthesis and electrochemical performances", *Electro. Acta*, **317**, 786-794 (2019).
36. G. Xi, X. Jiao, Q. Peng, and T. Zeng, "Anchored $CoCO_3$ on peeled graphite sheets toward high-capacity lithium-ion battery anode", *J. Mater. Sci.*, **56**, 10510-10522 (2021).
37. D. Kim, Y. Kim, and H. Kim, "Improved fast charging capability of graphite anodes via amorphous $Al_2O_3$ coating for high power lithium ion batteries", *J. Power Sources*, **422**, 18-24 (2019).
38. Y. Wang, "Coprecipitated 3D nanostructured graphene oxide–$Mn_3O_4$ hybrid as anode of lithium-ion batteries", *J. Mater. Res.*, **30**, 484-492 (2015).
39. D. Jang, S. Suh, H. Yoon, J. Kim, H. Kim, J. Baek, and H. Kim, "Enhancing rate capability of graphite anodes for lithium-ion batteries by pore-structuring", *Appl. Surf. Sci. Adv.*, **6**, 100168 (2021).
40. M. He, H. P. Zhou, G. Q. Ding, Z. D. Zhang, X. Ye, D. Cai, and M. Q. Wu, "Theoretical-limit exceeded capacity of the $N_2$+$H_2$ plasma modified graphite anode material", *Carbon*, **146**, 194-199 (2019).

41. F. Ding, W. Xu, D. Choi, W. Wang, X. Li, M. H. Engelhard, X. Chen, Z. Yan, and J. Zhang, "Enhanced performance of graphite anode materials by $AlF_3$ coating for lithium-ion batteries", *J. Mater. Chem.*, **22**, 12745 (2012).
42. S. Yehezkel, M. Auinat, N. Sezin, D. Starosvetsky, and Y. Ein-Eli, "Bundled and densified carbon nanotubes (CNT) fabrics as flexible ultra-light weight Li-ion battery anode current collectors", *J. Power Sources*, **312**, 109-115 (2016).
43. L. Li, C. Fan, B. Zeng, and M. Tan, "Effect of pyrolysis temperature on lithium storage performance of pyrolitic-PVDF coated hard carbon derived from cellulose", *Mater. Chem. Phys.*, **242**, 122380 (2020).